J Digit Imaging (2015) 28:594–603
DOI 10.1007/s10278-015-9784-6

A Quantification Method for Breast Tissue Thickness and Iodine Concentration Using Photon-Counting Detector

Seokmin Han

Published online: 24 February 2015

Abstract The purpose of contrast-enhanced digital mammography (CEDM) is to facilitate detection and characterization of the lesions in the breast using intravenous injection of an iodinated contrast agent. CEDM produces iodine images with gray levels proportional to iodine concentration at each pixel, which can be considered as quantification of iodine. While dual-energy CEDM requires an accurate knowledge of the thickness of compressed breast for the quantification, it is known that the accuracy of the built-in thickness measurement is not satisfactory. Triple-energy CEDM, which can provide a third image, can alleviate the limitation of dual-energy CEDM. If triple exposure technique is applied, it can lead to increased risk of motion artifact. An energy-resolving photon-counting detector (PCD) that can acquire multispectral X-ray images can reduce the risk of motion artifact. In this research, an easily implementable method for iodine quantification in breast imaging was suggested, and it was applied to the images of breast phantom with various iodine concentrations. The iodine concentrations in breast phantom simulate lesions filled with different iodine concentrations in the breast. The result shows that the proposed method can quantify the iodine concentrations in breast phantom accurately.

Keywords Breast · Digital mammography · Digital image processing

Introduction

X-ray mammography is still an important tool in screening and diagnostic examination for early detection of breast cancer, for it is known that mammography examinations improve survival rates for breast cancers. Recent advances in a digital X-ray detector provide digital mammography system, which also gives opportunities for early detection of breast cancer. For early detection of breast cancer, the visibility of breast masses in the mammogram is very important. However, the superposition of glandular structures causes relatively low contrast, which limits detectability of cancer [1]. To enhance detectability of breast cancer, dual-energy contrast-enhanced digital mammography (CEDM) has been used as a technique with potential to improve the detection of breast carcinomas, which involves intravenous injections of iodinated contrast media, in conjunction with mammography examination [2, 3]. Currently, CEDM is not used as a screening method due to iodine injection which causes discomfort of patients. However, it has been reported that CEDM can be an alternative screening method to breast MRI for a high-risk group [4, 5]. Thus, the method to improve detectability of cancer by iodine injection seems to have the potential to be more widely used.

A possible limitation of current dual-energy CEDM comes from the fact that overlapping normal breast tissue structures can obscure the detection of iodine, and that just two images provide the solution to the two-variable equation [6], while three variables that are required as the breast consists of three materials—adipose and glandular tissues and iodine. A priori knowledge of the breast thickness for each pixel is required to solve this problem using dual-energy CEDM. However, in many clinical mammography systems which employ a spring-loaded paddle, the physical thickness of the breast may not be uniform due to deformation and tilt of the compression paddle [7]. Furthermore, it is reported that the built-in thickness measurement is not accurate [8, 9], which can affect the performance. Triple-energy CEDM, which provides a third image, has been considered to overcome the necessity of thickness information.

S. Han (✉)
SAIT, Samsung Electronics, Samsung-ro, Youngtong-gu, Suwon-si, Kyunggi-do, South Korea
e-mail: seokmin.han@samsung.com

Triple-energy approaches have been suggested for CT, fluoroscopy, and mammography [10–15]. To apply triple-energy method to mammography, three images for three energy bins should be acquired. The three-energy bin approach sometimes requires three exposures. However, it does not mean that a high dose is required. For example, a dose of each exposure can be controlled to be about 1/3 mGy. Then, three exposures will give a total dose of 1 mGy, which is close to the normal dose of conventional mammography. If a triple-exposure technique is applied, it may lead to increased risk of motion artifact. An energy-resolving photon-counting detector (PCD), which can subdivide an incident X-ray spectrum into three energy bins, can provide triple-energy radiography, reducing risk of motion. In this research, an easily implementable method was proposed, which extends the method for dual-energy imaging to the method for triple-energy imaging, to generate the iodine image. It makes use of the calibration phantom image itself, rather than numerical calculation. The proposed method does not require the priori knowledge of the spectrum shape and the tissue attenuation, which can reduce the complexity of implementation. In terms of dose, imaging parameters were selected to meet the dose level of conventional mammography. It should be noted that this study is an extension of the author's previous research [16].

Method and Materials

Brief Background Scheme

When an imaged object does not contain k-edge contrast material, the transmitted intensity can be modeled as follows:

$$I_{\mathrm{tr}}(E_i) = \int_{E_i} S_o(E) e^{-\mu_{\mathrm{glan}}(E) t_{\mathrm{glan}} - \mu_{\mathrm{adi}}(E) t_{\mathrm{adi}}} dE, (i = 1, 2) \quad (1)$$

where I_{tr} is transmitted intensity, E_i is the ith photon energy spectrum, $S_o(E)$ is the incorporation of incident X-ray intensity and detector gain at photon energy E, $\mu_{\mathrm{glan}}(E)$ is the attenuation coefficient of glandular tissue at energy E, $\mu_{\mathrm{adi}}(E)$ is the attenuation coefficient of adipose tissue at energy E, t_{glan} is the thickness of glandular tissue, and t_{adi} is the thickness of adipose tissue. In Eq. 1, there are two unknown variables (t_{glan} and t_{adi}). Therefore, two measurements of the transmitted intensity at photon energy spectrum E_1 and E_2($I_{\mathrm{tr}}(E_1)$ and $I_{\mathrm{tr}}(E_2)$) are enough to solve Eq. 1. This concept can be illustrated in Fig. 1.

Two measurements I_1',I_2' of the target object, one for each energy bin, are mapped onto the corresponding surfaces of potential solutions; then, we can draw two lines on S_1 and S_2 as displayed in Fig. 1. All points on the drawn line of surface

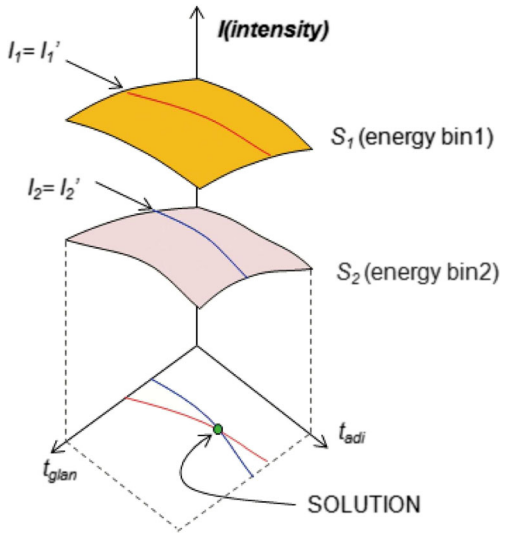

Fig. 1 Illustration of lines of two measurements (I_1,I_2) in a space consisting of t_{glan},t_{adi}, and intensity value. Lines are drawn on the accordant surfaces of energy bins 1 and 2 (S_1,S_2). The lines are projected onto a 2D plane consisting of (t_{glan},t_{adi})

S_1 have the same value, I_1'. Likewise, all points on the drawn line of S_2 have the value I_2'. In Fig. 1, lines of two measurements (I_1',I_2') are drawn on the accordant surfaces of energy bin 1 and energy bin 2 (S_1,S_2), respectively. As the lines are projected onto a 2D plane consisting of (t_{glan},t_{adi}), the line drawn on S_1 can be considered as a set of possible solutions to Eq. 1 at E_1. In the same way, the line drawn on S_2 can be considered as a set of possible solutions to Eq. 1 at E_2. If the two lines, which correspond to measurements I_1' and I_2' in energy bins E_1 and E_2, respectively, intersect at one point, then the corresponding material thicknesses at the point give the common solution to Eq. 1 in both E_1 and E_2. This problem corresponds to a two-dimensional (2D) case. The precise explanation of a 2D case is provided in [17].

If the target imaging object contains a k-edge contrast material, the practical relation expressed in Eq. 1 should be adjusted as follows [16]:

$$I_{\mathrm{tr}}(E_i) = \int_{E_i} S_o(E) e^{-\mu_{\mathrm{glan}}(E) t_{\mathrm{glan}} - \mu_{\mathrm{adi}}(E) t_{\mathrm{adi}} - \mu_I(E) t_I} dE, (i = 1, 2, 3) \quad (2)$$

where $\mu_{\mathrm{glan}}(E)$ is the attenuation coefficient of glandular tissue at energy E, $\mu_{\mathrm{adi}}(E)$ is the attenuation coefficient of adipose tissue at energy E, $\mu_I(E)$ is the attenuation coefficient of k-edge contrast agent (iodine) at energy E, t_{glan} is the thickness of glandular tissue, t_{adi} is the thickness of adipose tissue, and t_I is the thickness of iodine. In Eq. 2, there are three unknown variables (t_{glan}, t_{adi}, and t_I), and $I_{\mathrm{tr}}(E_1)$, $I_{\mathrm{tr}}(E_2)$, and $I_{\mathrm{tr}}(E_3)$, three measurements of the transmitted intensity at photon energy spectra E_1, E_2, and E_3, are enough to solve Eq. 2. For one

intensity measurement, three variables in Eq. 2 plot a surface in 3D space consisting of (t_{glan}, t_{adi}, and t_I). Likewise, three measurements, one for each energy bin, plot three surfaces. If a solution exists when $I_{tr}(E_1)=I'_1, I_{tr}(E_2)=I'_2, I_{tr}(E_3)=I'_3$, it means that the surfaces intersect at one point in the 3D space. This corresponds to an extension of a 2D case described in Eq. 1 to a 3D case.

Material Decomposition Using Reference Phantom

Constructing the Surface of Possible Solutions

For calibration, the calibration phantom images of three energy bins were acquired.

In Fig. 2, the calibration phantom is displayed. The phantom is designed to range in thickness from 2 to 9 cm so that they include a wide range of breast thicknesses. It also has the range in ratio of glandular and adipose material from 0 to 100 % at a particular thickness. Iodine equivalent slab phantom of a specific concentration is attached to the bottom of the calibration phantom. As the calibration phantom is composed of three materials, Eq. 2 can be applied to the phantom.

As can be seen in Fig. 2, while the calibration phantom has a continuous mixture of adipose and glandular equivalent tissue, its iodine equivalent tissue has discrete concentrations. Therefore, we have to estimate the effect of an arbitrary iodine concentration on the calibration phantom image using a few images of calibration phantoms with specific iodine concentration. Varying the concentration of iodine slab phantom, many calibration phantoms could be constructed, and each calibration phantom had its specific iodine concentration. Suppose we have three calibration phantoms with iodine concentrations of 0, 5, and 10 mg/ml, and three images for each calibration phantom, one for each energy bin, are acquired then, we have nine calibration phantom images. Considering the three images of the low-energy bin, each calibration phantom image has different pixel values at the same location. In the same way, a particular pixel value of an imaged object will correspond to different locations on the three phantom images. This is shown in Fig. 3a, b. In Fig. 3a, locations that correspond to a pixel value are marked on a low-energy calibration phantom image with 0 mg/ml concentration iodine slab. In Fig. 3b, locations that are marked on low-energy calibration phantom images with 0, 5, and 10 mg/ml iodine slabs are combined and drawn together to illustrate that a particular pixel value of an imaged object corresponds to different locations due to iodine concentration differences. Here, the locations appear to be three curves on the reference phantom. Each curve corresponds to each phantom with a specific iodine concentration.

Similarly, suppose we have infinitely many calibration phantoms with infinitely small increments in iodine concentration. Then, infinitely many curves will be drawn on the phantom, which will constitute a surface. In short, we can draw a surface in 3D space that interpolates those curves in

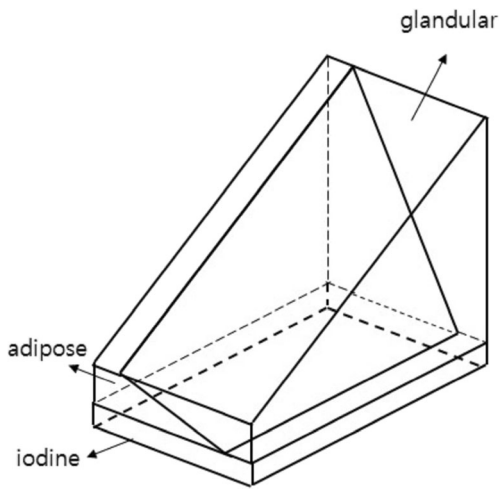

Fig. 2 A reference phantom with thickness variation and glandular rate variation. The phantom is designed to range in thickness from 2 to 9 cm so that they include a wide range of breast thicknesses. It also has the range in ratio of glandular and adipose materials from 0 to 100 % at a particular thickness. At the bottom, an iodine equivalent slab phantom is attached

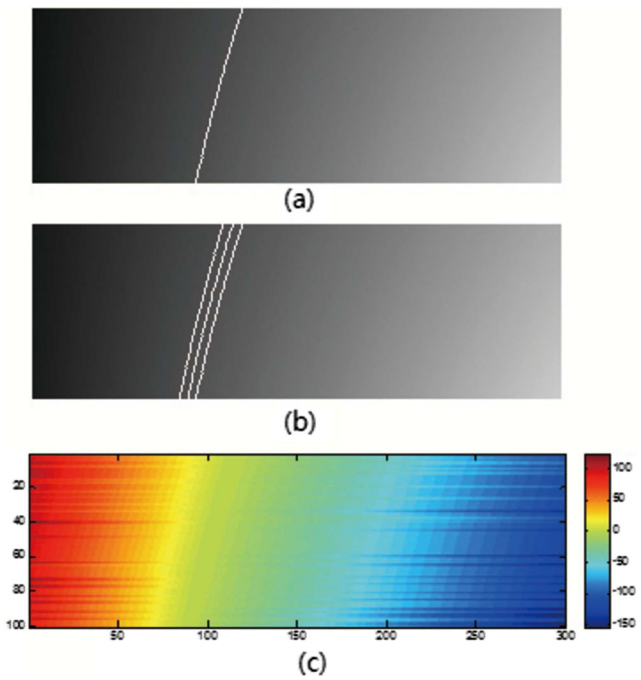

Fig. 3 In **a**, locations that correspond to a pixel value marked on a calibration phantom image with a 0-mg/ml iodine slab are drawn. In **b**, locations that are marked on calibration phantom images with 0, 5, and 10 mg/ml iodine slabs are combined and drawn together. **c** A surface is created, interpolating curves in **b**. The *colorbar* indicates the iodine concentration (mg/ml)

Fig. 3b for a pixel value. Various interpolation techniques can be used to plot the surface. In this study, a linear interpolation method was used. The surface drawn in 3D space is shown in Fig. 3c as a colormap. This surface corresponds to a set of possible solutions of (t_{glan}, t_{adi}, and t_f) to Eq. 2 in the low-energy bin (energy bin1). In the same way, surfaces in the middle-energy bin and high-energy bin can be also drawn for a pixel.

Combining the Constructed Surfaces

We can draw a surface in each energy bin for a pixel as shown in Fig. 4. Surfaces for the low-energy, middle-energy, and high-energy bin (S_1,S_2,S_3) are shown in Fig. 4a, b, c, respectively. Each surface has different shape. As explained in the background scheme section, three energy bin images are required to discriminate three materials. Similarly, if we combine the three constructed surfaces constructed in each energy bin, the three surfaces in 3D space intersect at one point if there exists a solution. The intersection point can be found by finding the minimum x of the following equation.

$$x = \{x | min_{x \in S_i} |S_1 - S_2| + |S_2 - S_3| + |S_3 - S_1|\}, (i = 1, 2, 3) \quad (3)$$

where $|\cdot|$ indicates absolute distance, S_i is the surface in the ith energy bin. In this study, the three energy bins (energy bins 1, 2, and 3) were used, and they can be considered the low-, middle-, and high-energy bins, respectively.

The location of the intersection point indicates the estimated iodine concentration, the estimated glandular tissue thickness, and the estimated adipose tissue thickness, which gives the solution to Eq. 2. Because the iodine slab phantoms of different concentrations have the same size (thickness and area), the variation of iodine concentration in the target object can be converted to the thickness variation at the same iodine concentration in the calibration phantom.

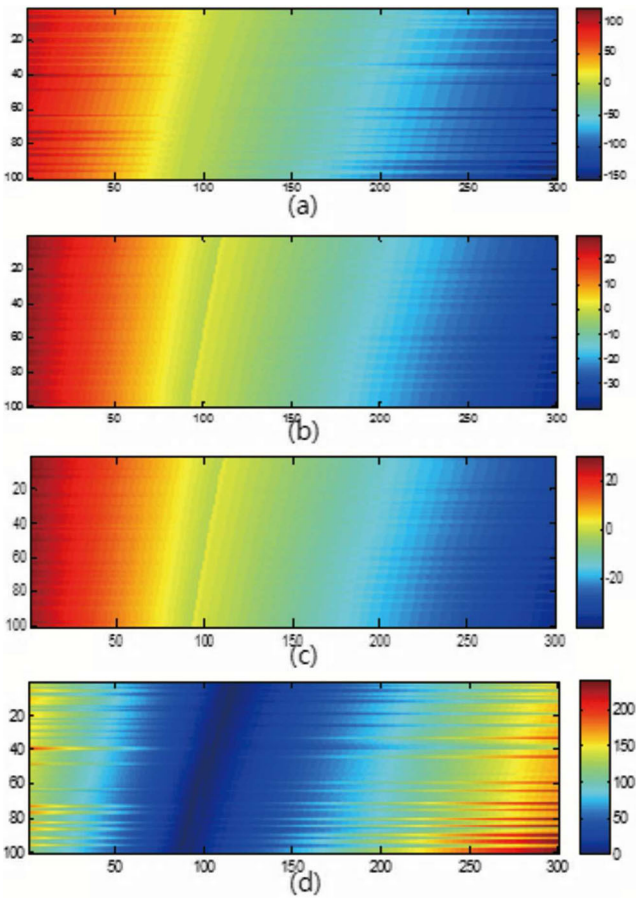

Fig. 4 **a** Created surface of energy bin 1 in 3D space, **b** surface of energy bin 2, **c** surface of energy bin 3. In **a**, **b** , and **c**, the *colorbar* indicates the iodine concentration (mg/ml). **d** Combined three surfaces from three energy bins. They intersect at one point (minimum point). The *colorbar* indicates the difference of iodine concentration among the surfaces in (**a**),(**b**),(**c**)

Experiments

This research aimed to quantify the concentration of iodine mass in breast phantom. For calibration, three calibration phantoms with iodine concentration of 0, 5, and 10 mg/ml were prepared. To simulate iodine mass in the real breast, eight cylindrical holes in one breast slab (Model 020, CIRS, Inc.) were made, and the holes were filled with materials that mimic the X-ray attenuation of various concentrations of iodine, which were also provided by CIRS. The iodine inserts have a cylindrical shape, 1 cm in diameter and 1 cm in height. The thickness (height) of iodine inserts is the same with that of one breast slab phantom. The iodine concentrations of iodine inserts were 4, 6, 8, and 10 mg/ml in pairs to fill eight holes in the slab phantom. One-cm thickness breast phantoms of random marbling were stacked on the breast slab phantom with iodine inserts. For example, four breast phantoms were stacked on the breast phantom with iodine inserts to make a 5-cm-thick phantom, and five phantoms were stacked on the phantom with iodine inserts to make a 6-cm-thick phantom. In Fig. 5, the breast slab phantom is shown.

For image acquisition, a proof-of-concept photon-counting mammography system was built using a pixelated CdTe PCD (made by DxRay, Inc., Northridge, CA, USA) and a X-ray tube (made by Varian X-Ray Products, Salt Lake City, UT, USA). The source to image distance (SID) of the system was 65 cm, like that of commercial mammography. The PCD can set four energy thresholds, and subsequently, it can have four energy bins. The X-ray tube has tungsten anode and an Ag 0.03-mm inherent filter. The images were acquired at 49kVp, 8mAs, and three energy bins were used (20–26, 26–30, 35–49 keV) as low-energy bin, middle-energy bin, and high-energy bin.

Fig. 5 Illustration of the breast slab phantom used in this research

After image acquisition of the breast phantoms, the proposed method was applied to the acquired images, and the concentrations of iodine inserts in the breast phantoms were quantified. It should be noted that the breast images and the estimated iodine concentrations were low-pass filtered to reduce noise since the goal of this research is to quantify the iodine concentration in breast mass, which is 1 cm in size. A Gaussian filter of 9×9 size was employed as the low-pass filter. For evaluation, the average value and the relative error of estimated iodine concentration were calculated in each region of interest (ROI). ROI is defined as the region of 5× 5 mm in each iodine insert, and the relative error is defined as

$$\text{relative error} = \sqrt{\frac{1}{n}\sum_{i=1}^{n}\left(\frac{I_c - I_s}{I_s}\right)^2} \times 100, \quad (4)$$

where I_c is the estimated iodine concentration, I_s is the desired concentration of iodine, and n is the number of pixels in ROI to calculate I_c and I_s. The meaning of relative error is the percentage of error in estimating the iodine concentration, normalized by the desired concentration and averaged over ROI. For example, suppose that the desired concentration is 8 mg/ml and the relative error is 25 % then the average estimation result should be 6 or 10 mg/ml. The mean value of total tissue thickness values of the breast slab phantoms was also quantified. The total tissue thickness indicates the sum of adipose tissue thickness and glandular tissue thickness. It was done to show that estimated iodine concentration does not depend on glandular ratio, considering that the breast thickness is the sum of adipose tissue and glandular tissue.

Results

Using the images of the reference calibration phantom, the proposed method was applied to the images of the breast slab phantoms with iodine inserts to estimate the iodine concentration. Concentrations of iodine inserts in 5, 6, and 7 cm breast phantoms were estimated and quantified by relative error, which is defined in Eq. 4, and the results are plotted in Figs. 8 and 9.

For illustration, the acquired low-energy image of a 5-cm-thick breast phantom with iodine inserts is displayed in Fig. 6a. In Fig. 6b, estimated iodine concentrations are presented as a colormap image. In Fig. 6c, an estimated tissue thickness map is presented as a colormap image. Tissue thickness is the sum of thicknesses of adipose tissue and glandular tissue. We can see that the background regions are about 5 cm in height, while the regions of iodine inserts are about 4 cm in height, regardless of iodine concentration. Considering that iodine inserts are 1 cm in height, the proposed method could quantify tissue thickness successfully. Even though glandular ratio varied, iodine concentration estimation was not affected, and the sum of glandular tissue and adipose tissue did not vary.

In Fig. 7a, estimated iodine concentrations of a 5-cm breast phantom are presented with a yellow centerline, and the profile of the iodine concentrations is shown in Fig. 7b. From the left, the true concentrations of iodine inserts are 4, 6, 8, and 10 mg/ml.

The estimated iodine concentrations were close to the true concentrations of iodine inserts as can be seen in Fig. 7b.

In Figs. 8 and 9, the results are shown in graphs. In Fig. 8a, the estimated iodine concentration denotes the average value of ROI in each iodine insert.

The standard deviation of each ROI was also calculated to show error bound in Fig. 8b, c, d. Considering the results shown in Fig. 8a, we can infer that the estimated iodine concentrations follow the desired values, regardless of breast thickness. R^2 values and the estimated trend lines were also displayed in Fig. 8b, c, d. An R^2 value larger than 0.9 means that the trend line is reliable.

However, the average value of each ROI seems to show some bias. In Fig. 8b, c, d, we can see that the error bound does not seem to depend much on the desired concentration. That seems to be related with the fact that the relative error was larger in 4-mg/ml cases. In Fig. 9, a 4-mg/ml case shows the largest relative error, which shows the combined effect of the average value and the standard deviation. As the concentration of iodine increases, the relative error shows a tendency to decrease. In Fig. 9, the trend line is drawn based on the data at 6, 8, and 10 mg/ml. The trend line shows large deviation at the data at 4 mg/ml. This seems to be related with the minimum detectable iodine concentration [24], which was 4 mg/ml in concentration. The total thickness values of the breast slab phantoms were also evaluated, and the results are summarized in Table 1. In Fig. 10b, the profiles of the estimated thickness of breast phantoms are displayed. We can see that the difference in thickness between the background region

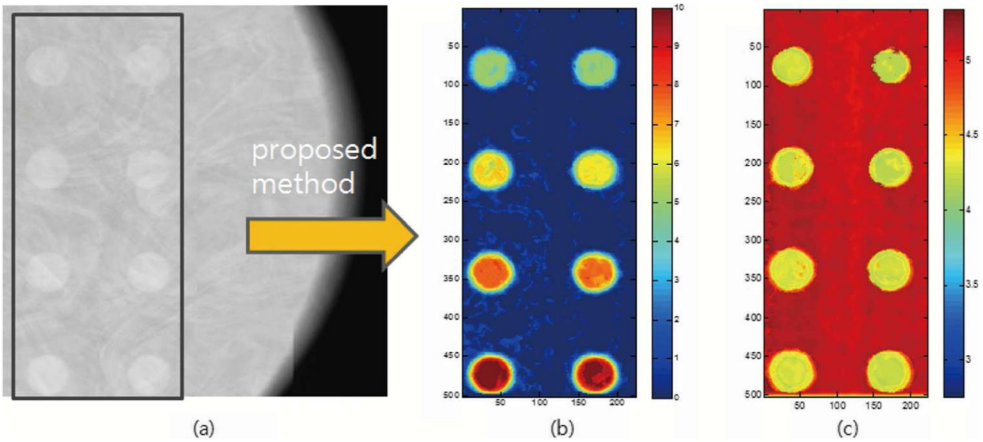

Fig. 6 **a** A low-energy image of a 5-cm breast phantom is displayed. Eight iodine lesions can be seen. From the *top*, iodine inserts have concentrations of 4, 6, 8, and 10 mg/ml. **b** Reconstructed iodine concentrations are presented. The *colorbar* implies the iodine concentration (mg/ml). **c** An estimated tissue thickness map is presented. The *colorbar* indicates the tissue thickness (cm)

and the region of iodine inserts is about 1 cm thickness, regardless of iodine concentration and phantom thickness.

The estimated mean glandular dose (MGD) for each case is shown in Table 2, following the dose calculation method by Dance [18, 19]. The breast thicknesses were 5, 6, and 7 cm.

Due to the random pattern of a breast phantom, the average glandular ratio could not be exactly calculated.

Thus, MGD was estimated assuming that the breast phantoms have 50 % glandular ratio. Because PCD was used, it was not necessary to acquire images several times to get a high-energy image or a low-energy image.

Just one exposure provided images at each energy bin.

Considering the results, the proposed method could quantify iodine in breast phantom using PCD.

Discussion

To facilitate detection and characterization of lesions in the breast, dual-energy imaging methods using an intravenous contrast medium have been suggested. However, the overlapping of normal breast tissue can limit the visibility of iodine in dual-energy imaging. While three variables are required as the breast consists of three materials, adipose and glandular

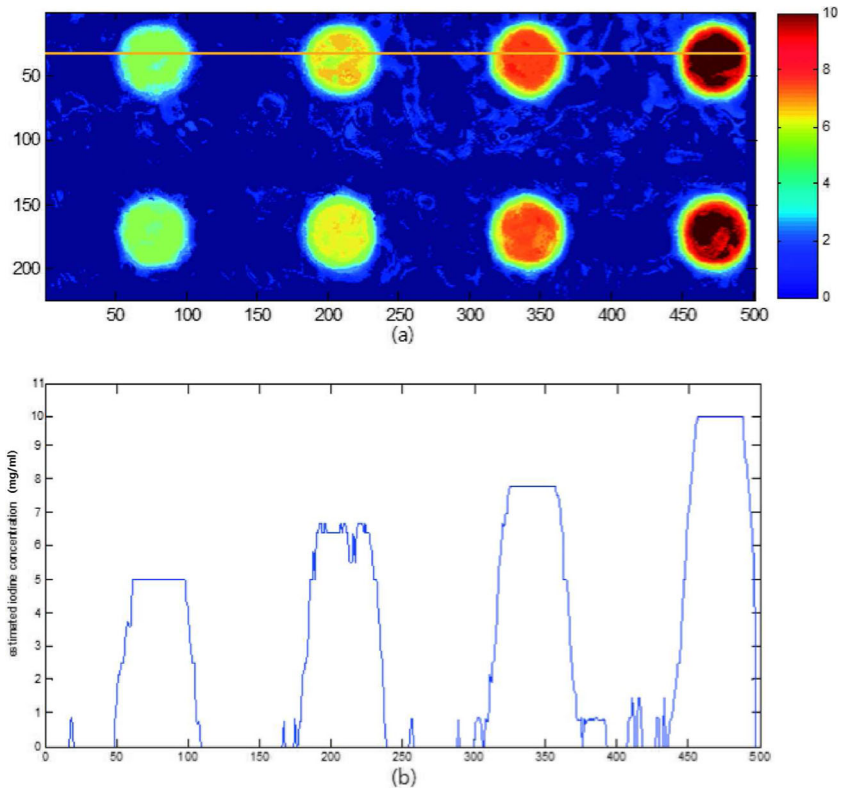

Fig. 7 **a** A low-energy image of the breast phantom is displayed. Four iodine lesions can be seen. From the *left*, iodine inserts have concentrations of 4, 6, 8, and 10 mg/ml. The *colorbar* indicates the iodine concentration (mg/ml). **b** Reconstructed iodine concentrations are presented

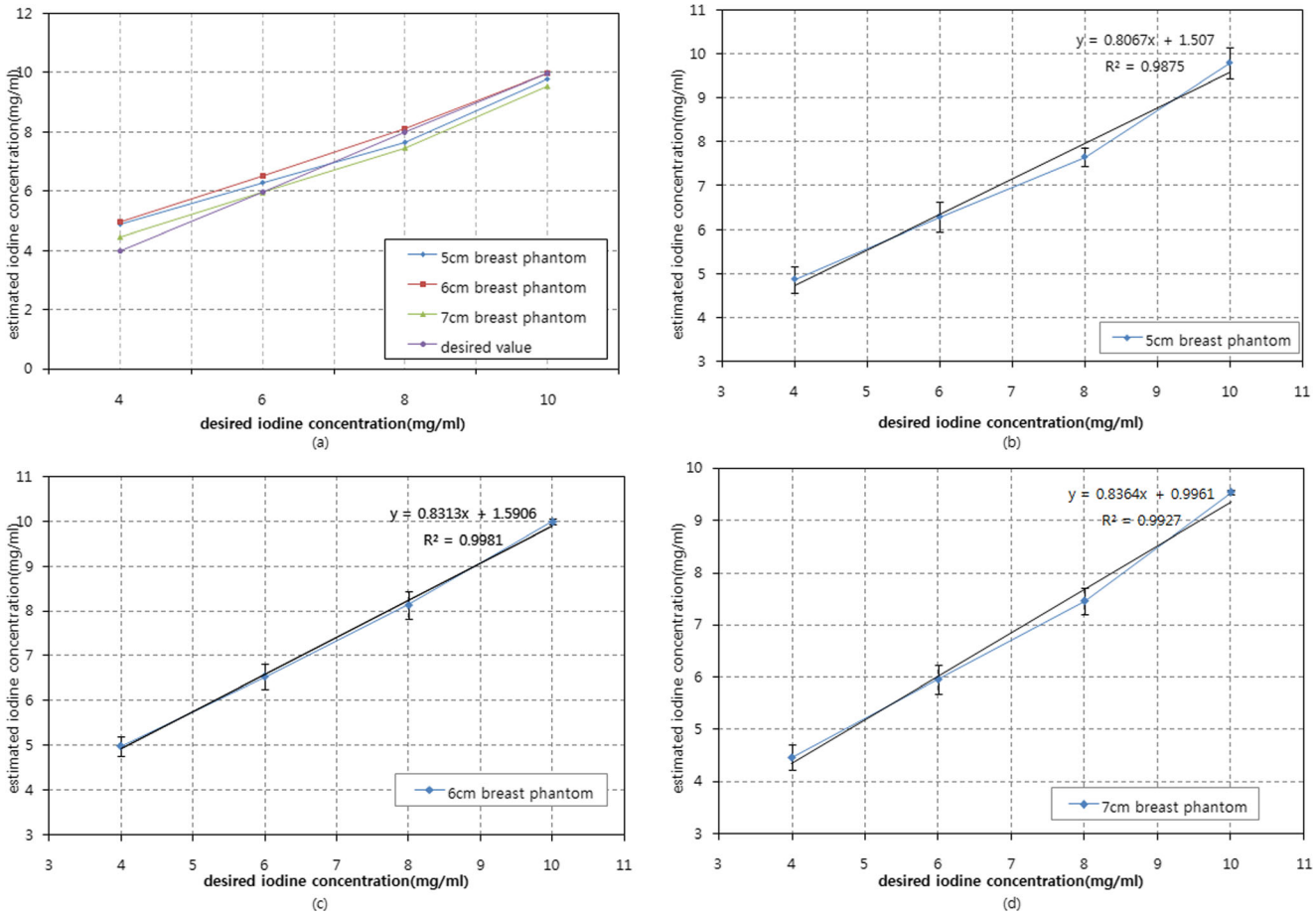

Fig. 8 **a** Comparison between the reconstructed mean concentrations and the true concentrations of iodine inserts in the phantom. Mean concentrations are plotted with *error bars* for **b** a 5-cm breast phantom, **c** a 6-cm breast phantom, and **d** a 7-cm breast phantom. In **b**, **c**, **d**, the estimated trend lines and R^2 values are also displayed

tissues and iodine, only two images are acquired to provide a solution to the two variable equations.

Furthermore, attenuation coefficients of a breast tissue-equivalent phantom, which is widely used for calibration, mimic the average value of attenuation coefficients of individual breast tissue [20]. This indicates that individual breast tissue shows variation of attenuation coefficient. For example, the attenuation coefficients of an individual glandular tissue

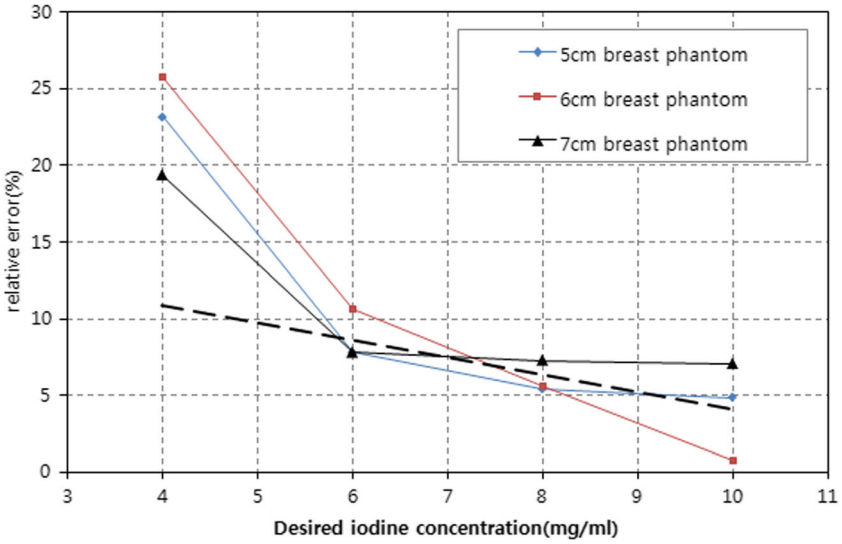

Fig. 9 A relative error of estimated iodine concentration. Relative error values show a tendency to decrease as iodine concentration increases. The *dotted line* indicates the trend calculated from the results at 6, 8, and 10 mg/ml

Table 1 Estimated total thickness at each thickness and concentration

	Background	4 mg/ml	6 mg/ml	8 mg/ml	10 mg/ml
Five slabs (5 cm)	5.1072	4.2453	4.2476	4.2844	4.2625
Six slabs (6 cm)	5.9609	5.1210	5.1462	5.1972	5.1399
Seven slabs (7 cm)	6.7842	5.9623	6.0135	6.0802	6.0620

Table 2 Estimated MGD (mGy) values at each thickness and each imaging parameter

Imaging condition	Five slabs (5 cm)	Six slabs (6 cm)	Seven slabs (7 cm)
49 kVp, 8 mAs, W/Ag	1.024	0.862	0.705

can be different from the average values because of hydration of the tissue, and the density of the breast tissue of a lean person can be different from that of an obese person [21–23]. There also exists considerable variation in the attenuation coefficients reported in the various studies [24]. To adaptively quantify the amount of contrast material in breast, a priori knowledge of the breast thickness for each pixel is required. However, it is also known that the built-in thickness measurement is not accurate in many clinical mammography systems which employ a spring-loaded paddle [8, 9]. Therefore, a triple-energy method is employed, which can provide a third image to overcome the limitation of the dual-energy method. Here, it is assumed that the attenuation coefficients of iodine do not have variation among individuals, for iodine is not a biological material. The images of the calibration phantom with iodine concentrations of 0, 5, and 10 mg/ml were acquired. Breast phantoms used in this study included iodine inserts of 4, 6, 8, and 10 mg/ml in concentration. Considering the previous researches related with the iodine concentration in a blood vessel [25–30], it was assumed that the concentration of iodine ranges from 4 to 10 mg/ml in the breast. An amount of 4 mg/ml was set as the lowest concentration considering the minimum iodine concentration used for k-edge subtraction mammography [25]. As for the shape of lesions, the cylinder-like lesion used in this research will give clear sharp edges with a well-defined volume. If lesions were like spiculated spheres, things might be somewhat different. It would be more difficult to detect lesions because of irregular shape and thickness. However, it should be noted that the proposed method is focused more on quantifying the concentration of iodine than on detecting lesions. In fact, in

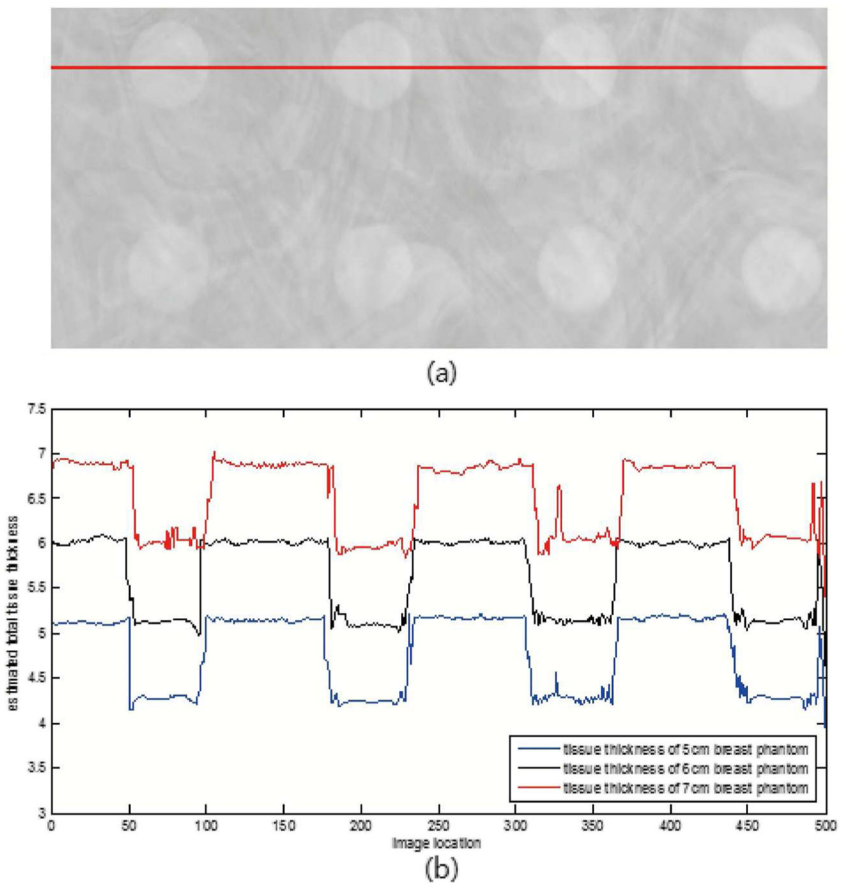

Fig. 10 Estimated thickness of 5-, 6-, and 7-cm breast phantoms at the *red centerline*. The thickness of iodine inserts (1 cm) is excluded

CEDM, it is assumed that the relatively high concentration sites of iodine correspond to lesions. To estimate the iodine concentration and to compare the result with the desired value, we should have the perfect knowledge about the lesion shape. If the lesions had a spiculated shape, it would surely be more relevant to a real clinical situation. However, it would also be very difficult to know the desired value of iodine concentration perfectly due to its irregular shape. It seems that a cylinder-like phantom, used in this research, is appropriate for the estimation and the comparison with the desired value, for it has uniform thickness. If the lesions were spiculated sphere and the perfect knowledge about the desired thickness and the concentration of the lesions were given, this research could be more relevant to a realistic situation. Thus, we consider that the future work to deal with more realistic lesion simulations is necessary.

In terms of the size of an iodine insert, the iodine inserts are designed to be 1 cm in diameter and 1 cm in height. It is known that the size of stage 1 breast cancer is less than 2 cm in diameter [31]. Thus, it seems that a 1-cm-thick cylinder phantom, which is used in this research, can be used to test the detectability of iodine in a lesion, considering the size of stage 1 breast cancer.

The result shown in Fig. 10 indicates that the proposed method could estimate the breast tissue thickness as well as iodine concentration. The estimated tissue thickness in this study is the sum of thicknesses of adipose tissue and glandular tissue. The estimated thicknesses were about 5.11, 5.96, and 6.78 cm in the background region and about 4.25, 5.15, 6.02 cm in the iodine insert region for 5-, 6-, and 7-cm breast phantoms, respectively. The difference between thicknesses in the background region and thicknesses in the iodine insert region, which was about 0.8 cm, was caused by iodine inserts. The difference seems to slightly increase as total thickness increases. It may come from the fact that as total thickness increases, the signal from iodine inserts gets relatively reduced.

The limitation of this research is the use of artificial phantoms which may be different from biological tissues. The calibration phantoms and breast phantoms contain known materials and mixtures. However, biological tissues have variations in materials, mixtures, and densities. In some cases, an unexpected variation occurs in biological tissues. In those cases, the materials and their mixtures in biological tissues will be decomposed into the basis materials which were used in this study. In other words, the biological tissues with variations are projected into the three basis materials, leading to possible errors in tissue quantification. However, fortunately, an iodine contrast agent is not a biological material, and it has little variation in attenuation coefficients even when the variation in biological tissues occurs. If the variation in attenuation coefficients occurs, it is from the biological materials, and it affects the estimation of biological material. Due to k-edge, the characteristic of iodine is not affected much by the variation in attenuation coefficients among individuals.

It should be noted that this study is a preliminary study to use PCD for the quantification of iodine and tissue thickness in mammography. PCD optimization was not complete, especially for selecting optimal energy threshold values. If optimal energy threshold values for PCD are set, it may produce better results [32]. It is our ongoing research to optimize PCD and to apply the proposed method to biological tissues.

Conclusions

Possible limitations of current dual-energy CEDM come from the overlapping of breast tissue structures, and the fact that two images acquired with dual-energy CEDM provide a solution for two materials—adipose and glandular tissues. To alleviate the limitations of dual-energy CEDM, triple-energy CEDM, which can provide a third image, was used. A photon-counting detector could provide triple-energy radiography with reduced risk of motion artifact. An iodine quantification method for breast imaging was suggested, and it was applied to breast phantom with different iodine concentrations. The result shows that the proposed method could quantify the concentration of iodine inserts in breast phantom accurately, which simulate lesions filled with different iodine concentrations in the breast.

References

1. Thomas R. Nelson, Laura I. Cerviño, John M. Boone, and Karen K. Lindfors: Classification of breast computed tomography data. Medical Physics, 2008
2. Clarisse Dromain, Corinne Balleyguier, Ghazal Adler, Jean Remi Garbay, Suzette Delaloge: Contrast-enhanced digital mammography. European Journal of Radiology, 2009
3. John M. Lewin, Pamela K. Isaacs, Virginia Vance, Fred J. Larke: Dual-Energy Contrast enhanced Digital Subtraction Mammography: Feasibility. Radiology, October 2003
4. Clarisse Dromain, Fabienne Thibault, Felix Diekmann, Eva M. Fallenberg, Roberta A. Jong, Marcia Koomen, R. Edward Hendrick, Anne Tardivon and Alicia Toledano: Dual-energy contrast-enhanced digital mammography: initial clinical results of a multireader, multicase study. Breast Cancer Research, 2012
5. Maxine Jochelson: Contrast-Enhanced Digital Mammography. Radiologic Clinics of North America, 2014
6. Yu Zou and Michael D. Silver: Analysis of Fast kV-switching in Dual Energy CT using a Prereconstruction Decomposition Technique. Proceeding of SPIE, March 2008
7. Serghei Malkov, Jeff Wang, Karla Kerlikowske, Steven R. Cummings, and John A. Shepherd: Single x-ray absorptiometry method for the quantitative mammographic measure of fibroglandular tissue volume. Medical Physics, 2009

8. Albert H. Tyson, Gordon E. Mawdsley, and Martin J. Yaffe: Measurement of compressed breast thickness by optical stereoscopic photogrammetry. Medical Physics, 2009
9. A. Burch and J. Law: A method for estimating compressed breast thickness during mammography. British Journal of Radiology, 1995
10. P.V. Granton, S.I. Pollmann, N.L. Ford, M. Drangova, and D.W. Holdsworth: Implementation of dual- and triple-energy cone-beam micro-CT for postreconstruction material decomposition. Medical Physics, 2008
11. J. P. Schlomka, E. Roessl, R. Dorscheid, S. Dill, G. Martens, T. Istel, C. Bäumer, C. Herrmann, R. Steadman, G. Zeitler, A. Livne and R. Proksa: Experimental feasibility of multi-energy photon-counting K-edge imaging in pre-clinical computed tomography. Physics in Medicine and Biology, 2008
12. Markus Firsching, Patrick Takoukam Talla, Thilo Michel, Gisela Anton: Material resolving X-ray imaging using spectrum reconstruction with Medipix2. Nuclear Instruments and Methods in Physics Research Section A, 2008
13. P. S. Yeh, A. Macovski, and W. Brody: Noise analysis in isolation of iodine using three energies. Medical Physics, 1980
14. F. Kelcz. and C.A. Mistretta: Absorption-edge fluoroscopy using a three-spectrum technique. Medical Physics, 1976.
15. S. Puong, P. Milioni de Carvalho, and S. Muller: Triple-Energy Contrast Enhanced Digital Mammography. Proc. of SPIE, 2010
16. Seokmin Han, Dong-Goo Kang, Sunghoon Kang, Younghun Sung: Quantitative breast imaging using photon counting detector. Proc. SPIE. 8668, Medical Imaging, 2013
17. Seokmin Han, Dong-Goo Kang: Tissue cancellation in dual energy mammography using a calibration phantom customized for direct mapping. IEEE Transactions on Medical Imaging, 2014
18. D.R. Dance, C.L. Skinner, K.C. Young, J.R. Beckett, C.J. Kotre: Additional factors for the estimation of mean glandular breast dose using the UK mammography dosimetry protocol. Physics in Medicine and Biology, 2000
19. D.R. Dance: Monte Carlo calculation of conversion factors for the estimation of mean glandular breast dose. Physics in Medicine and Biology, 1990
20. William P. Argo, Kathleen Hintenlang, and David E. Hintenlang: A tissue-equivalent phantom series for mammography dosimetry. Journal of Applied Clinical Medical Physics, Vol 5, No 4, 2004
21. Grant E. van der Ploeg, Robert T. Withers, and Joe Laforgia: Percent body fat via DEXA: comparison with a four-compartment model. Journal of Applied Physiology, February 2003
22. Angelo Pietrobelli, Zimian Wang, Carmelo Formica, and Steven B. Heymsfield: Dual-energy X-ray absorptiometry: fat estimation errors due to variation in soft tissue hydration. Americal Journal of Physiology Endocrinology and Metabolism, May 1998
23. J.T.M. Jansen,W.J.H. Veldkamp, M.A.O. Thijssen, S. van Woudenberg, and J. Zoetelief: Method for determination of the mean fraction of glandular tissue in individual female breasts using mammography. Physics in Medicine and Biology, 2005
24. Christopher E Tromans, Mary R Cocker and Sir Michael Brady: Quantification and normalization of x-ray mammograms. Physics in Medicine and Biology, 2012
25. P. Baldelli,A. Bravin, C. Di Maggio, G. Gennaro, A. Sarnelli, A. Taibi, M. Gambaccini: Evaluation of the minimum iodine concentration for contrast-enhanced subtraction. Physics in Medicine and Biology, 2006
26. Robert A. Kruger: Estimation of the diameter of and iodine concentration within blood vessels using digital radiography devices. Med Phys, 1981
27. T. P. Fuerst, M. S. Van Lysel: Measurement of absolute blood iodine concentration during digital subtraction ventriculography. Med Phys, 1993
28. Felix Diekmann, Ulrich Bick: Tomosynthesis and contrast-enhanced digital mammography: recent advances in digital mammography. Eur Radiol, 2007
29. Masatoshi Saito: Dual-energy approach to contrast-enhanced mammography using the balanced filter method: spectral optimization and preliminary phantom measurement. Med Phys, 2007
30. Robert Leithner, Thomas Knogler and Peter Homolka: Development and production of a prototype iodine contrast phantom for CEDEM. Phys Med Biol, 2013
31. S. Eva Singletary, Craig Allred, Pandora Ashley, Lawrence W. Bassett, Donald Berry, Kirby I. Bland, Patrick I. Borgen, Gary Clark, Stephen B. Edge, Daniel F. Hayes, Lorie L. Hughes, Robert V.P. Hutter, Monica Morrow, David L. Page, Abram Recht, Richard L. Theriault, Ann Thor, Donald L. Weaver, H. Samuel Wieand and Frederick L. Greene: Revision of the American Joint Committee on Cancer Staging System for Breast Cancer. Journal of Clinical Oncology, July 2002
32. E. Fredenberg, M. Hemmendorff, B. Cederström, M. Åslund, and M. Danielsson: Contrast-enhanced spectral mammography with a photon-counting detector. Medical Physics, 2010